Agility and Accuracy: Phased Array vs Single-Element Ultrasonic Testing in the Characterization of Barely Visible Impact Damage in CFRP Laminates

Rachel E. Van Lear, Daniel P. Pulipati, Pruthul Kokkada Ravindranath, Trevor J. Fleck, and David A. Jack

Baylor University
100 Research Pkwy
Waco, Texas 76704
David_Jack@baylor.edu

ABSTRACT

Damage of carbon-fiber laminates due to impact in-service or during maintenance is often difficult to evaluate visually. Unlike metallic systems, the real damage to a laminate is often beneath the surface and cannot be quantified using optical or surface inspection methods, often being termed barely visible. Sub-surface, non-destructive testing methods, such as ultrasonic testing, are useful in detecting the three-dimensional nature of barely visible impact damage. To quickly detect and quantify such damage, there has been an increasing industrial push towards utilizing phased array ultrasonic testing methods. This relatively recent adoption of phased array ultrasonic testing poses the need for determining the speed and accuracy of the scanning method for impact damage as compared to the more established but time consuming conventional single-element transducer ultrasonic testing techniques. This study compares these two ultrasonic testing techniques by impacting 22-layer carbon fiber laminates using a drop tower with 16J, 18J, and 20J energies, ultrasonically scanning the resulting damage area, and comparing the quantification of the impact damage zone along with the scanning time between techniques.

Keywords: Carbon Fiber-Reinforced Polymer, Barely Visible Impact Damage, Phased Array Ultrasonic Testing

INTRODUCTION

Laminated composites are increasingly integrated into innovative designs and applications due to their beneficial, anisotropic properties, but the lack of methods to quantify laminate impact damage spark a need for improved algorithms and advanced scanning methods using non-destructive testing techniques (NDT). With an excellent strength-to-weight ratio, damping and high stiffness qualities, and corrosion resistance, composites are utilized in automotive, aerospace, renewable energy, and various other industries to push the boundaries of fuel efficiency and performance [1]–[12]. However, these advanced materials are not indestructible. Due to the anisotropic nature of composites, the possibility of defects and susceptibility to damage is different than metals. In composites, manufacturing defects such as foreign object debris, voids, porosity, out-of-plane wrinkles, in-plane wrinkles, and ply misalignment pose a risk to the overall structural performance, as does impact damage. The detection and quantification of impact damage caused in-service or during maintenance is of the upmost importance for predicting the overall lifecycle of the composites. This study aims at detecting and quantifying barely visible impact damage (BVID) in carbon fiber composites [7], [8], [13]. BVID can be defined as damage that cannot be discovered by visual inspection with normal lighting at a distance of 5 feet from the composite [14], [15]. The reduction in part performance from this type of damage, coupled with its difficulty of detection, emphasizes the need for NDT methods to be constructed to detect damage that would otherwise be missed by visual inspections.

BVID is a major concern for composite laminates since they are particularly susceptible to impacts due to a lack of fibers in the normal direction [16], [17]. When an impact occurs on the surface of a laminate, the normal force causes the laminate to bend, leading to tension on the bottom half of the laminate [18]–[20]. This causes fiber fracture and delamination to propagate from the back half of the laminate towards the upper half, with the largest damage areas often occurring within the lower half of the laminate [12], [21], [22]. BVID is often induced in-service from debris or during maintenance via unexpected tool drop and results in a decrease in the residual compressive strength and stability of composite structures [1], [2], [4], [5], [15], [18], [20], [21], [23]–[25]. Often the effects of BVID on the residual compressive properties of composites are studied via compression after impact (CAI) testing, as done by the authors in the precursor to this study with the same laminate layup [1]. The importance of efficient NDT techniques is emphasized with the possibility of BVID resulting in reduced structural performance or failure of composites and the inadequacy of visual inspections for its detection [7], [26].

The main focus of this study is the use of ultrasonic testing (UT) techniques for BVID detection and quantification, but various NDT techniques have been used in the qualification of composites in manufacturing or in-service [12], [26], [27]. NDT techniques such as computed tomography, vibrothermography, infrared thermography, and shearography have all been used for BVID detection [12], [28], [29], but UT is comparatively inexpensive [3], [30] and allows for the reduction of inspection setup time via the in-situ scanning of parts for BVID [10], [31], [32]. Within the category of UT, two main transducers will be the focus of this study: conventional single-element (SE) and linear phased array (PA). Linear PA transducers contain multiple elements that can be used to take data at several points without moving the transducer, allowing for PA UT to scan with an optimized path and requiring less time than SE UT to scan the same area. A common concern with the use of quick PA UT over SE UT transducers is an increase of noise at high frequency and large depth due to material microstructure [33]. This study aims to satisfy this concern by measuring the accuracy of PA against its conventional SE counterpart.

Continuing the work of Blandford *et al.* [2], [3], this investigation compares the mature SE UT technique of three dimensional BVID detection and quantification with that of the linear PA UT technique using the same automated BVID detection tool from that of Van Lear *et al.* [1]. There have been many studies on the detection and/or quantification of BVID via conventional UT techniques [1]–[3], [12], [19], [20], as well as via phased array UT techniques [4], [5], [8], [9], [13], [22], [28], [29], [34]. Nonetheless, the comparison of BVID detection between SE and PA UT techniques in not only the detection, but also the quantification of BVID can be limited to studies of Katunin *et al.* [35], [36], based on the results of this literature review. While most studies from Katunin *et al.* focus on hybrid techniques, combining NDT technologies to greater understand composite damage [35], [37], Wronkowicz-Katunin *et al.* is most relevant to this study regarding the comparison of SE and PA UT. In Wronkowicz-Katunin *et al.*, the process for the automatic detection of BVID via SE and PA UT data is similar to that of this study, but when comparing the quantification of damage of the two techniques, the equivalent damage diameters of the 20J coupon has a difference of up to roughly 5 mm [36]. This current study can be seen as an extension to the work of Katunin *et al.*, where the quantified damage is obtained using automated methods and the maximum difference between SE and PA detected damage is approximately 1.40 mm with a standard deviation of ± 0.43 mm for the fifteen coupons studied at differing impact energies, while also comparing the scan time of each technique.

Overall, this study focuses on comparing single-element and linear phased array ultrasound inspection techniques of barely visible impact damage in carbon fiber reinforced polymer (CFRP) laminates. Examining the damage from three impact energies (16J, 18J, and 20J), BVID was able to be detected and quantified throughout the coupons to find the maximum effective damage diameters of each of the fifteen coupons with both SE and PA techniques. Both techniques produced congruent measurements, but PA UT was able to scan each coupon with a 95% reduction in time as compared to SE UT, confirming the agility and accuracy of PA for not only BVID detection, but quantification as well.

MATERIALS AND METHODS

Manufacturing Details

The carbon fiber laminates for this investigation were manufactured in-house using a [Woven/-30/+60/0/90/-60/+60/-30/+30/0/90]s layup pattern from 7" x 10" pre-preg sheets. Two pre-preg types were used during the layup: a Toray T300 plain weave fabric for the two outer layer face-sheets and a Toray T700 unidirectional fabric for the remaining lamina. Both systems used the same 250F Resin System from Rock West Composites. In an effort to decrease spalling from impact, the laminate layup included woven face-sheets in which the woven fabric cells restricted delaminations from growing along the outer face-sheets (see e.g., [17]). These woven face-sheets reduce the overall surface damage, but result in laminate damage difficult to identify visually. After the 22 sheets of the pre-preg were stacked, the CFRP laminates were cured via a Carver Auto Series Plus hot press at a temperature of 135°C for 3 hours and 30 minutes as per the manufacturer recommended cure cycle. Once the laminates were cured, two 4" x 6" coupons were cut out of each laminate with a WAZER Standup waterjet cutter.

Drop Weight Impact Testing

For this study, coupons were impacted at 16J, 18J, and 20J impact energies and resulted in BVID, as seen in Figure 1. Surface damage can only be observed if one is shown exactly where to investigate in these coupons. There are various fabrication markings on the laminates shown in Figure 1, but the only marking of relevance in the present context is the silver square. This region indicates the zone containing the damage along with the full scan window for inspection. The highest impact energy, 20J, produced large delaminations within the coupons that were easily detectable via UT. Impact energies were then incrementally decreased to more difficult-to-detect delamination sizes until 16J. The smallest impact energy, 16J, was chosen based on a previous study [1], which was limited by the load cell availability during CAI Testing. The available 100 kN load cell allowed for a maximum residual compressive strength of that from a 16J impacted coupon with the same layup as this current study, only permitting breakage of higher impact energies.

All impacts were performed in accordance with American Society for Testing and Materials (ASTM) standard D7136 [16]. An Instron 9450 Drop Weight Impact Testing Machine was utilized during testing with a lightweight impactor, 3 kg additional mass, and a 16 mm diameter hemispherical striker tip. Five coupons of the same layup were impacted at each level of energy, totaling fifteen coupons in this study. A plot of force as a function of time for the impact event for each of the coupons can be seen in Figure 3.

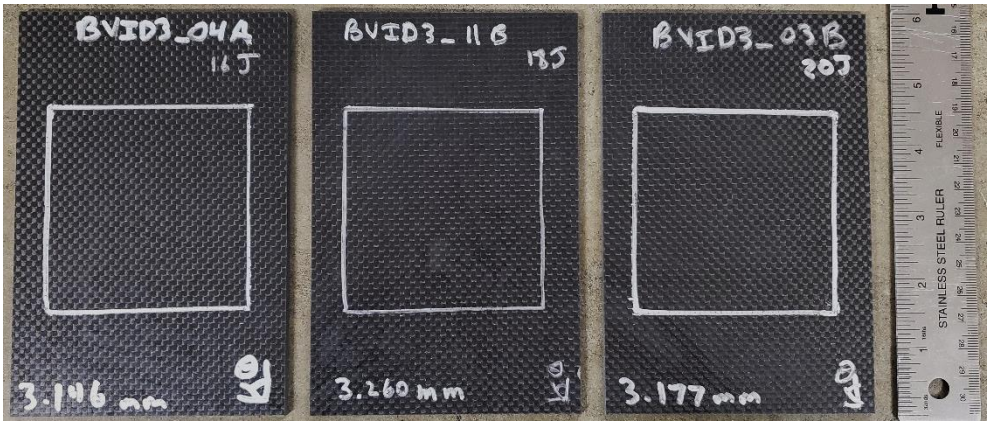

(a) **(b)** **(c)**

Figure 1: Coupons with BVID impacted with (a) 16J, (b) 18J, and (c) 20J energies. Observe that damage cannot be identified visually from the respective coupons.

Ultrasonic Testing Evaluation of Damage

To evaluate the impact damage, coupons were scanned using conventional single-element and linear phased array transducers. Both techniques utilized an Olympus FOCUS PX system and a custom ultrasonic immersion system. For the single-element UT technique, a 10 MHz conventional Olympus focused transducer was used with a data collection resolution of 0.2 mm. During data collection, stepper motors moved the transducer in a raster pattern throughout the 76.2 mm by 76.2 mm scanning region, which resulted in a scan time of 45 minutes.

For the phased array UT technique, a 10 MHz linear array Olympus transducer with 64 elements was used with a skew angle of 90° and an aperture of 16 elements. In data collection, the 0.2 mm scan resolution was the same as the conventional technique. The stepper motors moved the transducer in an overlapping, two swipe pattern. Due to the overlapping nature of the raster pattern, the index resolution was found to be 0.3 mm, two times the distance between the two swipes. The PA UT technique resulted in an average scan time of less than 2 minutes.

After scan data had been collected in each case, the data was saved as an Olympus proprietary *.fpd file. An in-house MATLAB script was used to read the a-scans from the raw data file, which used Focus Data for the conversion. The a-scans were subsequently smoothed using a spatial gaussian filter and used to generate c-scan images (Figure 2(b)). The MATLAB script was then used to detect and automatically quantify damage throughout the coupon. This script required the selection of damage depth from a b-scan taken from the middle of the scan, as seen in Figure 2(a). In this figure, bounds containing the topmost damage and the first instance of the largest damage were selected for the script to parse through in the b-scans. The script then divided the selected damage depth into 18 layers for analysis. Once the damage depth was selected and divided, the tool also required user selection of the damage from the maximum c-scan, as seen in Figure 2(b). Once the area of interest was selected, the custom script binarized the c-scan image for each divided layer based on a user defined threshold. The effective damage diameter was then measured, and the damage profile of each layer was saved. The maximum effective damage diameter is then saved, and a 3D plot of the damage geometry for each layer of the coupon was created, as seen in Figure 2(c). The colors shown in Figure 2(c) are denoted for easy visualization between the layers.

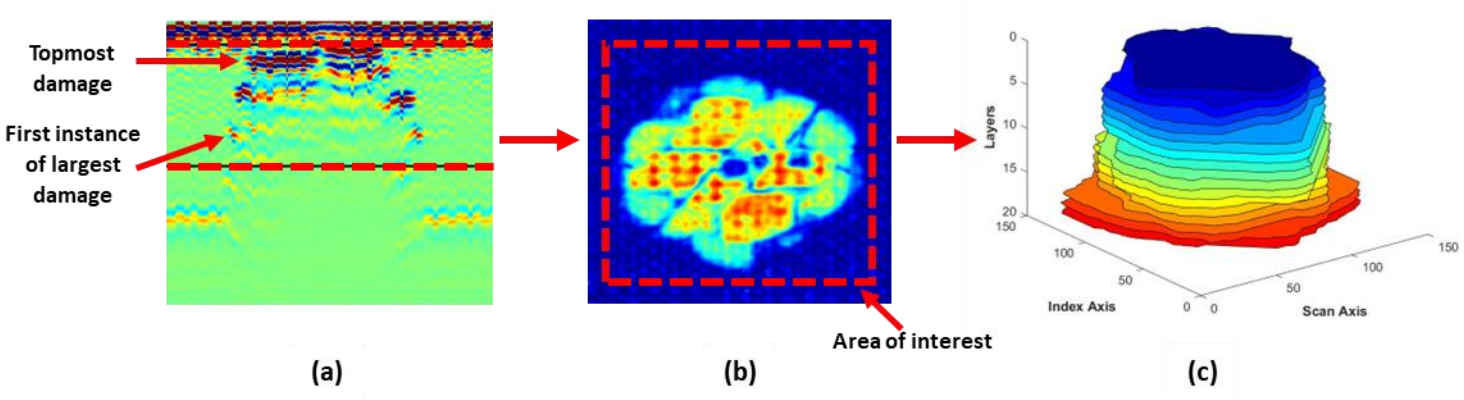

Figure 2: (a) A b-scan used for the selection of the damage depth. (b) A maximum c-scan used to select the damage area of interest. (c) A 3D plot of the impact damage throughout the coupon.

RESULTS AND DISCUSSION

Impact Testing

In Figure 3, impact tests show a similar grouping of force-time curves for the 16J, 18J, and 20J impact energies. Notice the tight grouping of damage profiles by impact energy, and there is a monotonic increase in the force curve as the impact energy increases. The authors note that there is one outlier in the data set for one of the five 20J impacted coupons that has a force profile less than that of the 18J impact. That outlier is kept within the presented data set for completeness, but future studies will seek to identify if that behavior can be duplicated. Additionally, an expected correlation between impact energy and peak force is confirmed from the figure.

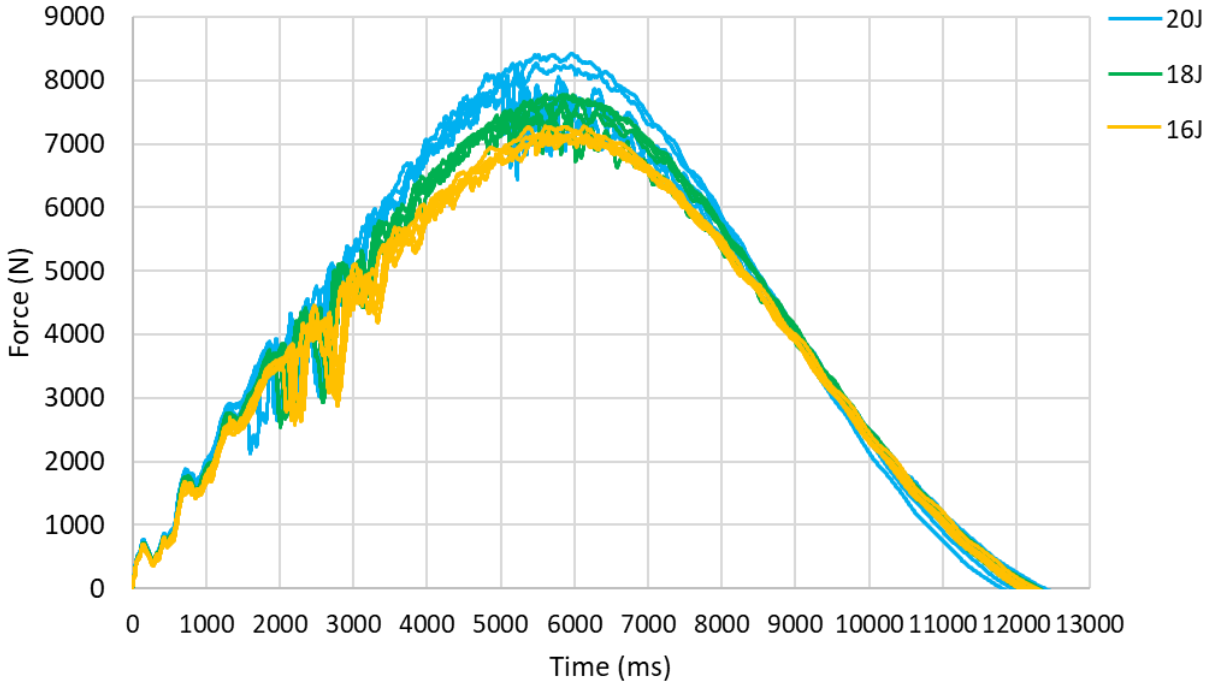

Figure 3: Impact force as a function of time from drop tower impact testing.

Comparison Between Characterization of Impact Damage

As seen in Table 1, the quantified damage of individual coupons is shown to be similar for both single-element and phased array UT results. In fact, nearly half of the coupons have less than a percent difference variation in effective damage diameters between SE UT and PA UT. All coupons have less than a millimeter difference between the two damage measurements, with the exception of Coupon #12, which was impacted with 20J and had a difference of 1.40 mm and a percent difference of 4.55%. It can also be observed that the results in Table 1 show that with an increase in impact energy the maximum effective damage diameter also linearly increases. For both the conventional single-element and linear phased array damage diameter measurements, both linear and logarithmic regressions were performed, with a logarithmic regression fitting performed to

$$d = a\ln(I_E) + b \qquad \textbf{(Eq. 1)}$$

where d is the damage diameter, I_E is the impact energy, and a and b are fitting coefficients. Both data sets favored a linear regression in the relationship between impact energy and damage diameter, with an R^2 value of 0.99 for SE UT and 0.97 for PA UT when performing a linear regression and an R^2 value of 0.98 for SE UT and 0.96 for PA UT for the logarithmic fitting.

Table 1: Comparison of conventional single-element and linear phased array damage analysis.

	Conventional Single-Element	*Linear Phased Array*		
Impact Energy	**Max Effective Damage Diameter (mm)**	**Max Effective Damage Diameter (mm)**	**Difference between diameters (mm)**	**Percent Difference**
16 J				
Coupon #1	26.76	26.81	0.04	0.16%
Coupon #2	26.53	27.40	0.87	3.24%
Coupon #3	27.14	27.22	0.08	0.29%
Coupon #4	25.61	26.44	0.84	3.22%
Coupon #5	25.61	25.57	0.04	0.16%
18 J				
Coupon #6	28.29	28.64	0.35	1.23%
Coupon #7	28.62	28.54	0.08	0.28%
Coupon #8	27.82	27.96	0.14	0.49%
Coupon #9	27.51	27.63	0.12	0.44%
Coupon #10	27.94	27.11	0.83	3.01%
20 J				
Coupon #11	29.50	29.53	0.02	0.08%
Coupon #12	30.03	31.43	1.40	4.55%
Coupon #13	30.74	30.15	0.59	1.93%
Coupon #14	29.82	29.05	0.77	2.61%
Coupon #15	29.91	29.27	0.64	2.17%

The results in Table 1 are further highlighted in Figure 4, which show similar damage measurements between the single-element and phased array UT techniques. The maximum effective damage diameters are plotted against the reported peak impact energies from the drop weight impact test for each coupon. Each coupon within an impact energy grouping is represented by a color. The SE UT damage measurement is represented by a solid triangle, while the PA UT damage measurement of the same coupon is denoted by a hollow square of the same color. As seen in Table 1, this plot also shows a positive correlation between impact energy and the resulting effective damage diameter of the impacted coupon.

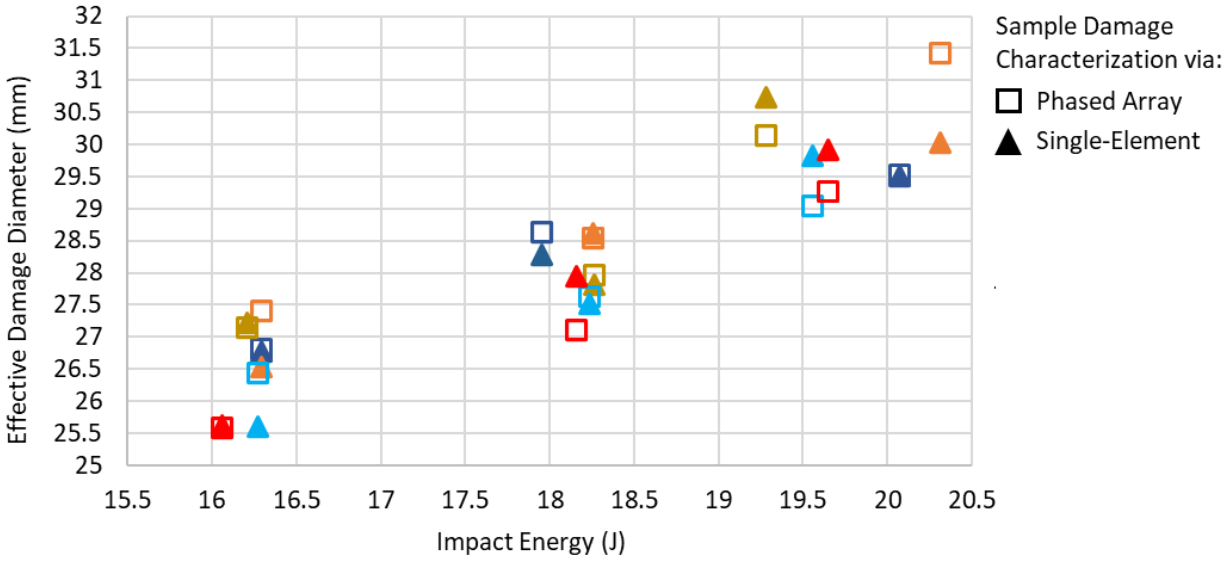

Figure 4: A plot of effective damage diameter vs impact energy. Shapes with matching colors and with the same impact energies are associated with the same coupon. Effective damage diameters found via phased array and single-element ultrasound techniques are relatively congruent.

As seen in Figure 5, 3D plots of damage from both single-element (Figure 5(a)) and phased array (Figure 5(b)) UT techniques for the same 16J impacted coupon show a relatively similar damage profile for most of the impact damage past the topmost layers. It is to be noted that the index axis scales are different in Figure 5 due to the conventional single-element and linear phased array techniques having differing index resolutions. In contrast, the scan resolutions for both techniques are 0.2 mm, which translates into the scan axes having the same scale for both SE and PA plots.

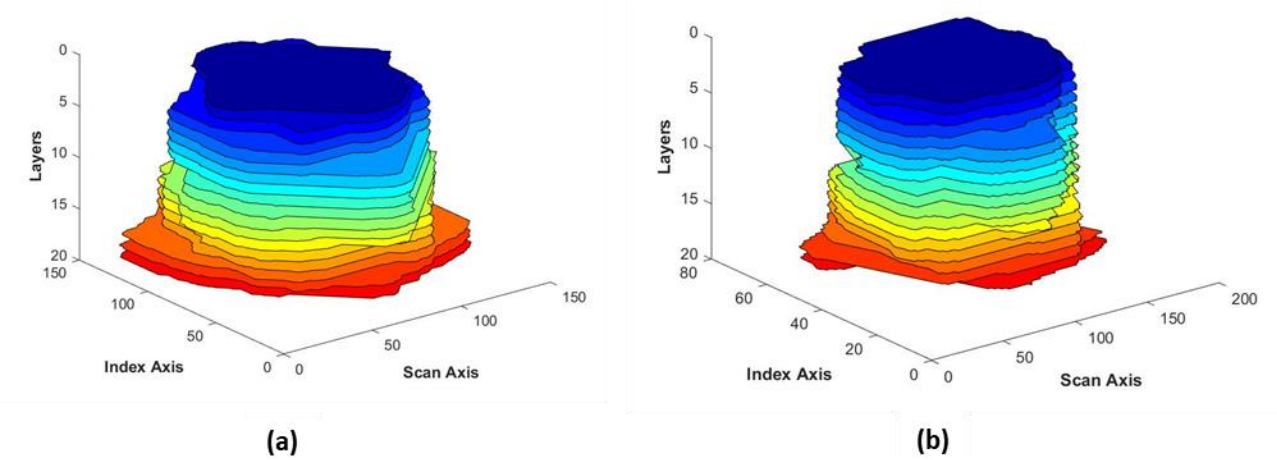

(a) (b)

Figure 5: (a) A 3D plot of damage throughout a 16J impacted coupon characterized via a conventional single-element transducer. (b) A 3D plot of damage throughout the same 16J impacted coupon characterized via a linear phased array transducer.

CONCLUSION

This study demonstrates that phased array ultrasonic testing can be used to quantify barely visible impact damage with nearly the same accuracy as conventional single-element techniques, within a 5% difference, but with a 95% reduction of inspection time from 45 to 2 minutes. This increased agility that phased array allows is invaluable for in-situ scanning of large areas with an arguably similar accuracy in the detection and quantification of BVID in carbon fiber laminates. Future work includes building on this study to quantify the accuracy of PA UT against X-ray CT imaging. In addition, future work will include phased array ultrasound inspection using beam steering to allow for a more robust three-dimensional picture of BVID.

ACKNOWLEDGEMENTS

The authors offer a special thanks to Verifi Technologies LLC for funding this study at Baylor University.

REFERENCES

[1] R. E. Van Lear, P. Kokkada Ravindranath, D. P. Pulipati, T. J. Fleck, and D. A. Jack, "Impact Damage Detection using Ultrasound and its Effect on Strength for CFRP Laminates," in *ASNT Research Symposium Conference Proceedings*, Jun. 2023.

[2] B. M. Blandford, "Nondestructive inspection and quantification of carbon fiber laminates for barely visible impact damage and adhesive layer thickness measurements.," Thesis, 2020. Accessed: May 19, 2023. [Online]. Available: https://baylor-ir.tdl.org/handle/2104/11022

[3] B. M. Blandford and D. A. Jack, "High resolution depth and area measurements of low velocity impact damage in carbon fiber laminates via an ultrasonic technique," *Compos. Part B Eng.*, vol. 188, p. 107843, May 2020, doi: 10.1016/j.compositesb.2020.107843.

[4] M. A. Perez, L. Gil, and S. Oller, "Non-destructive testing evaluation of low velocity impact damage in carbon fiber-reinforced laminated composites," *Ultragarsas Ultrasound*, vol. 66, no. 2, Art. no. 2, Jul. 2011, doi: 10.5755/j01.u.66.2.526.

[5] I. García-Moreno, M. Á. Caminero, G. P. Rodríguez, and J. J. López-Cela, "Effect of Thermal Ageing on the Impact Damage Resistance and Tolerance of Carbon-Fibre-Reinforced Epoxy Laminates," *Polymers*, vol. 11, no. 1, Art. no. 1, Jan. 2019, doi: 10.3390/polym11010160.

[6] V. Santhanakrishnan Balakrishnan and H. Seidlitz, "Potential repair techniques for automotive composites: A review," *Compos. Part B Eng.*, vol. 145, pp. 28–38, Jul. 2018, doi: 10.1016/j.compositesb.2018.03.016.

[7] B. Wang, S. Zhong, T.-L. Lee, K. S. Fancey, and J. Mi, "Non-destructive testing and evaluation of composite materials/structures: A state-of-the-art review," *Adv. Mech. Eng.*, vol. 12, no. 4, p. 1687814020913761, Apr. 2020, doi: 10.1177/1687814020913761.

[8] H. Towsyfyan, A. Biguri, R. Boardman, and T. Blumensath, "Successes and challenges in non-destructive testing of aircraft composite structures," *Chin. J. Aeronaut.*, vol. 33, no. 3, pp. 771–791, Mar. 2020, doi: 10.1016/j.cja.2019.09.017.

[9] G. P. Malfense Fierro and M. Meo, "Nonlinear elastic imaging of barely visible impact damage in composite structures using a constructive nonlinear array sweep technique," *Ultrasonics*, vol. 90, pp. 125–143, Nov. 2018, doi: 10.1016/j.ultras.2018.05.016.

[10] E. Duernberger, C. MacLeod, D. Lines, C. Loukas, and M. Vasilev, "Adaptive optimisation of multi-aperture ultrasonic phased array imaging for increased inspection speeds of wind turbine blade composite panels," *NDT E Int.*, vol. 132, p. 102725, Dec. 2022, doi: 10.1016/j.ndteint.2022.102725.

[11] H. Taheri and A. A. Hassen, "Nondestructive Ultrasonic Inspection of Composite Materials: A Comparative Advantage of Phased Array Ultrasonic," *Appl. Sci.*, vol. 9, no. 8, Art. no. 8, Jan. 2019, doi: 10.3390/app9081628.

[12] E. Jost, D. Moore, B. Blandford, D. Jack, and C. Saldana, "Nanofocus X-ray computed tomography and ultrasonic inspection of barely visible impact damage in carbon fiber reinforced polymers," *Rev. Prog. Quant. Nondestruct. Eval.*, no. 0, Art. no. 0, Dec. 2019, Accessed: Jun. 12, 2023. [Online]. Available: https://www.iastatedigitalpress.com/qnde/article/id/8675/

[13] M. A. Caminero, I. García-Moreno, G. P. Rodríguez, and J. M. Chacón, "Internal damage evaluation of composite structures using phased array ultrasonic technique: Impact damage assessment in CFRP and 3D printed reinforced composites," *Compos. Part B Eng.*, vol. 165, pp. 131–142, May 2019, doi: 10.1016/j.compositesb.2018.11.091.

[14] A. Fawcett and G. Oakes, "Boeing Composite Airframe Damage Tolerance and Service Experience," 2006.

[15] R. Talreja and N. Phan, "Assessment of damage tolerance approaches for composite aircraft with focus on barely visible impact damage," *Compos. Struct.*, vol. 219, pp. 1–7, Jul. 2019, doi: 10.1016/j.compstruct.2019.03.052.

[16] "Standard Test Method for Measuring the Damage Resistance of a Fiber-Reinforced Polymer Matrix Composite to a Drop-Weight Impact Event." https://www.astm.org/d7136_d7136m-15.html (accessed Jan. 23, 2023).

[17] C. Evci and M. Gülgeç, "An experimental investigation on the impact response of composite materials," *Int. J. Impact Eng.*, vol. 43, pp. 40–51, May 2012, doi: 10.1016/j.ijimpeng.2011.11.009.

[18] S. Takahashi, S. Kobayashi, I. Tomáš, L. Dupre, and G. Vértesy, "Comparison of magnetic nondestructive methods applied for inspection of steel degradation," *NDT E Int.*, vol. 91, pp. 54–60, Oct. 2017, doi: 10.1016/j.ndteint.2017.06.001.

[19] G. A. O. Davies and X. Zhang, "Impact damage prediction in carbon composite structures," *Int. J. Impact Eng.*, vol. 16, no. 1, pp. 149–170, Feb. 1995, doi: 10.1016/0734-743X(94)00039-Y.

[20] M. A. Caminero, I. García-Moreno, and G. P. Rodríguez, "Damage resistance of carbon fibre reinforced epoxy laminates subjected to low velocity impact: Effects of laminate thickness and ply-stacking sequence," *Polym. Test.*, vol. 63, pp. 530–541, Oct. 2017, doi: 10.1016/j.polymertesting.2017.09.016.

[21] S. M. García-Rodríguez, J. Costa, A. Bardera, V. Singery, and D. Trias, “A 3D tomographic investigation to elucidate the low-velocity impact resistance, tolerance and damage sequence of thin non-crimp fabric laminates: effect of ply-thickness,” *Compos. Part Appl. Sci. Manuf.*, vol. 113, pp. 53–65, Oct. 2018, doi: 10.1016/j.compositesa.2018.07.013.
[22] E. Panettieri, D. Fanteria, M. Montemurro, and C. Froustey, “Low-velocity impact tests on carbon/epoxy composite laminates: A benchmark study,” *Compos. Part B Eng.*, vol. 107, pp. 9–21, Dec. 2016, doi: 10.1016/j.compositesb.2016.09.057.
[23] B. M. Blandford, “Nondestructive Inspection and Quantification of Carbon Fiber Laminates for Barely Visible Impact Damage and Adhesive Layer Thickness Measurements,” Ph.D., Baylor University, United States -- Texas. Accessed: Feb. 01, 2023. [Online]. Available: https://www.proquest.com/docview/2408507218/abstract/57F82E8B48747A1PQ/1
[24] C. Nageswaran, C. R. Bird, and R. Takahashi, “Phased array scanning of artificial and impact damage in carbon fibre reinforced plastic (CFRP),” *Insight Non-Destr. Test. Cond. Monit.*, vol. 48, no. 3, pp. 155–159, Mar. 2006, doi: 10.1784/insi.2006.48.3.155.
[25] X. C. Sun and S. R. Hallett, “Failure mechanisms and damage evolution of laminated composites under compression after impact (CAI): Experimental and numerical study,” *Compos. Part Appl. Sci. Manuf.*, vol. 104, pp. 41–59, Jan. 2018, doi: 10.1016/j.compositesa.2017.10.026.
[26] R. Raišutis and O. Tumšys, “Application of Dual Focused Ultrasonic Phased Array Transducer in Two Orthogonal Cross-Sections for Inspection of Multi-Layered Composite Components of the Aircraft Fuselage,” *Materials*, vol. 13, no. 7, Art. no. 7, Jan. 2020, doi: 10.3390/ma13071689.
[27] B. R. Loyola, K. J. Loh, V. La Saponara, J. C. Chen, and T. M. Briggs, “COMPARATIVE STUDY OF NON-DESTRUCTIVE DAMAGE EVALUATION METHODOLOGIES FOR CFRP LOW VELOCITY IMPACT DAMAGE,” in *Navigating the Global Landscape for the New Composites*, Oct. 2012.
[28] Y. He, S. Chen, D. Zhou, S. Huang, and P. Wang, “Shared Excitation Based Nonlinear Ultrasound and Vibrothermography Testing for CFRP Barely Visible Impact Damage Inspection,” *IEEE Trans. Ind. Inform.*, vol. 14, no. 12, pp. 5575–5584, Dec. 2018, doi: 10.1109/TII.2018.2820816.
[29] C. Garnier, M.-L. Pastor, F. Eyma, and B. Lorrain, “The detection of aeronautical defects in situ on composite structures using Non Destructive Testing,” *Compos. Struct.*, vol. 93, no. 5, pp. 1328–1336, Apr. 2011, doi: 10.1016/j.compstruct.2010.10.017.
[30] T. E. Preuss and G. Clark, “Use of time-of-flight C-scanning for assessment of impact damage in composites,” *Composites*, vol. 19, no. 2, pp. 145–148, Mar. 1988, doi: 10.1016/0010-4361(88)90725-2.
[31] N. J. Blackman, “Evaluation of carbon fiber laminates via the use of pulse-echo ultrasound to quantify ply-stack orientation and manufacturing defects.,” Thesis, 2021. Accessed: Jun. 19, 2023. [Online]. Available: https://baylor-ir.tdl.org/handle/2104/11715
[32] I. Khan and D. A. Jack, “Characterization of Sub-surface Wrinkles Within a Laminated Composite Using a Novel Phased Array Ultrasonic Scanning Technique Incorporating a Portable Nozzle and Robotic Arm.”
[33] A. Velichko, “Quantification of the Effect of Multiple Scattering on Array Imaging Performance,” *IEEE Trans. Ultrason. Ferroelectr. Freq. Control*, vol. 67, no. 1, pp. 92–105, Jan. 2020, doi: 10.1109/TUFFC.2019.2935811.
[34] X. Wang, J. He, W. Guo, and X. Guan, “Three-dimensional damage quantification of low velocity impact damage in thin composite plates using phased-array ultrasound,” *Ultrasonics*, vol. 110, p. 106264, Feb. 2021, doi: 10.1016/j.ultras.2020.106264.
[35] A. Katunin, A. Wronkowicz-Katunin, and K. Dragan, “Impact Damage Evaluation in Composite Structures Based on Fusion of Results of Ultrasonic Testing and X-ray Computed Tomography,” *Sensors*, vol. 20, no. 7, Art. no. 7, Jan. 2020, doi: 10.3390/s20071867.
[36] A. Wronkowicz-Katunin, A. Katunin, and K. Dragan, “Reconstruction of Barely Visible Impact Damage in Composite Structures Based on Non-Destructive Evaluation Results,” *Sensors*, vol. 19, no. 21, Art. no. 21, Jan. 2019, doi: 10.3390/s19214629.
[37] A. Katunin, K. Dragan, T. Nowak, and M. Chalimoniuk, “Quality Control Approach for the Detection of Internal Lower Density Areas in Composite Disks in Industrial Conditions Based on a Combination of NDT Techniques,” *Sensors*, vol. 21, no. 21, Art. no. 21, Jan. 2021, doi: 10.3390/s21217174.